Experimental investigations and thermodynamic calculations of the interface reactions between ceramic moulds and Ni-based single-crystal superalloys: Role of solubility of Y in the LaAlO3 phase

Wang, Hang ; Shang, Genfeng; Liao, Jinfa; Yang, Bin; Yuan, Chen

DOI:
10.1016/j.ceramint.2018.01.192

Document Version
Peer reviewed version

Citation for published version (Harvard):
Wang, H, Shang, G, Liao, J, Yang, B & Yuan, C 2018, 'Experimental investigations and thermodynamic calculations of the interface reactions between ceramic moulds and Ni-based single-crystal superalloys: Role of solubility of Y in the LaAlO3 phase', *Ceramics International*, vol. 44, no. 7, pp. 7667-7673. https://doi.org/10.1016/j.ceramint.2018.01.192

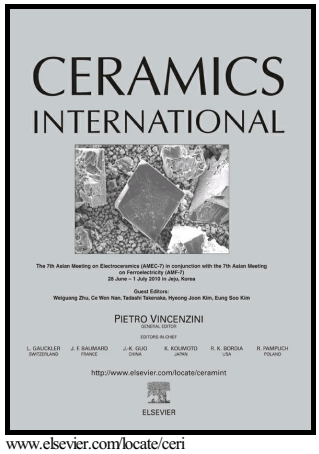

www.elsevier.com/locate/ceri

Experimental investigations and thermodynamic calculations of the interface reactions between ceramic moulds and Ni-based single-crystal superalloys: Role of solubility of Y in the $LaAlO_3$ phase

Hang Wang, Genfeng Shang, Jinfa Liao, Bin Yang, Chen Yuan

PII: S0272-8842(18)30205-0
DOI: https://doi.org/10.1016/j.ceramint.2018.01.192
Reference: CERI17324

To appear in: *Ceramics International*

Received date: 10 November 2017
Revised date: 21 January 2018
Accepted date: 22 January 2018

Cite this article as: Hang Wang, Genfeng Shang, Jinfa Liao, Bin Yang and Chen Yuan, Experimental investigations and thermodynamic calculations of the interface reactions between ceramic moulds and Ni-based single-crystal superalloys: Role of solubility of Y in the $LaAlO_3$ phase, *Ceramics International,* https://doi.org/10.1016/j.ceramint.2018.01.192

Experimental investigations and thermodynamic calculations of the interface reactions between ceramic moulds and Ni-based single-crystal superalloys: Role of solubility of Y in the $LaAlO_3$ phase

Hang Wang[1], Genfeng Shang[2], Jinfa Liao[2], Bin Yang[1*], Chen Yuan[3**]

1: Institute of Engineering Research, Jiangxi University of Science and Technology, Ganzhou 341000, China

2: School of Materials Science and Engineering, Jiangxi University of Science and Technology, Ganzhou 341000, China

3: School of Metallurgy and Materials, University of Birmingham, Birmingham B15 2TT, U.K.

*: yangbin65@126.com

**: c.yuan@bham.ac.uk

Abstract: It is commonly recognised that more reactive elements contained in Ni-based superalloy result in more-severe interfacial reactions, and thus more inclusions formed at the interface. However, the present work revealed that with rare-earth elements, specifically 0.24 wt.% La+Y added to Ni-based superalloys, the interfacial reaction (~5 μm in thickness) between the ceramics and metal was retarded compared to the case of 0.12 wt.% Y (~10 μm in thickness). Scanning electron microscopy, focused ion-beam transmission electron microscopy, and X-ray photoelectron spectroscopywere used to characterise the microstructure at the interface. Thermodynamic calculations of the Gibbs free energies of interfacial reactions were conducted. Experimental and theoretical results show that the solubility of Y in the $LaAlO_3$ phase (>3.4 at.%) hinders interfacial reactions.

Keywords: Ceramic mould; Ni-based superalloys; Interfacial reaction; Rare-earth elements; Thermodynamic calculations

1. Introduction

Ni-based superalloys are a type of metallic material with excellent oxidation resistance, corrosion resistance, and mechanical properties at elevated temperatures; they have been used for over 50 years to produce turbine blades in aerospace and gas turbines [1]. Complex geometries with very thin areas are always applied to the turbine blades in order to achieve good thermal dissipationand other advantages. Thus, investment casting is always employed to manufacture Ni-based single-crystal turbine bladesusingceramic moulds [2]. Silica-based ceramic moulds are often used as mouldmaterials thathave high bending strength and low deflection. However, during the casting process, interfacial reactions occur between the silica-based ceramic moulds and molten Ni because of the presence of reactive elements, such as Al [3-6], Cr [7-9], and Hf [10-13]. Interfacial reactions easily cause inclusions that are difficult to remove. Therefore, alumina with higher stability than silica is suggested as a mould material to retard interfacial reactions [14]. However, the issue still exists with the addition of a series of minor additives: rare earth elements (REEs).

Trace amounts of REEs are often added to remove impurities (such as sulphur) and improve the performance of oxidation resistance and creep resistance [7,8]. REEs are so reactive that Xue [15] found severe interfacial reactions between yttrium and silica-based moulds during casting. Ford et al. [16] tried to develop improved low-reactivity prime coats for blade moulds along with a viable, tight-dimensional-control yttrium oxide core body. Harris and Wahl [17] later reported the internal surface microstructure following single-crystal casting of CMSX-4® (SLS) [La+Y] with a silica-based core body, showing minimal reactivity.

Most of the mentioned research works focused on the interfacial reaction between REEs and silica-based moulds, but so far there are few reports on the interfacial reaction between REEs and alumina-based moulds. Nevertheless, interfacial reaction is inevitable for alumina, because REEs such as Y and La are much more reactive than Al. The Gibbs free energies of formation for the reactions $Al_2O_3 + 2Y \rightarrow Y_2O_3+2Al$ and $Al_2O_3 + 2La \rightarrow La_2O_3+2Al$ are −30~−70 kJ/mol at temperatures lower than 2000 °C [18]. In the present work, therefore, interfacial reactions between

alumina-based moulds and Y/Y+La-containing single-crystal Ni-based superalloys were investigated, by both experimental investigations and thermodynamic calculations.

When calculating the Gibbs free energies of ceramics, the solubility of a third element is sometimes neglected. This is due to mixed ionic and covalent ceramic bonds, resulting in a dense crystal structure that makes it quite difficult to dissolve any other elements [19]. However, some ceramics exhibit quite high solubility, such as Y in the $LaAlO_3$ phase (~ 5 at.%) and La in the $Y_4Al_2O_9$ phase (~ 3at.%) [20]. This will have a significant impact on the Gibbs free energies for the ceramics, so solubility must be taken into account while calculating the Gibbs free energy of the reactions. Although this increases the difficulty of the thermodynamic calculations, a CALPHAD (CALculation of PHAse Diagram) can provide an effective solution for the approach [21]. An identical thermodynamic model is used for each phase according to the crystal structure, and thermodynamic parameters are optimised to fit thermodynamic and phase equilibria data. As long as a set of self-consistent parameters is available, the Gibbs free energy of a ceramic phase with solubility such as $(La,Y)AlO_3$ can be obtained.

Therefore, in the present work, different phases were determined for the reactions of Y/Y+La and ceramic moulds. Thermodynamic calculations were carried out to calculate the Gibbs free energies of formation of different ceramic phases with and without Y/La solubility, and theoretical calculation results were compared with the experiments to provide explanations for the experimental observations.

2. Experiment

2.1 Alloy preparation

A second-generation single-crystal Ni-based superalloy was chosen with Y and La additionsin the present work. Alloys A and B included 0.12% Y and 0.12% Y+0.12% La (in wt.%), respectively. Nominal compositions of the two alloys are listed in Table 1. The purities of all the raw materialswere all 99.99 wt.% except Hf being 99.95 wt.%. Raw materials Co, Cr, Al, W, Mo, Ta were from Yuqing Materials Co.,

Shanghai; Hf was from Guangguang Materials Co., Guangdong; Re was from KETE China Rhenium Co., Hunan; La and Y were from Qiandong Rare Earth Group, Ganzhou; Ni was from Jinchuan Group, Gansu.

Table 1: Nominal compositions of the two alloys.

Alloy	Co	Cr	Al	W	Mo	Ta	Hf	Re	Y	La	Ni	Note
A	7.5	7.0	6.2	5.0	1.5	6.5	0.15	3.0	0.12	-	Bal.	wt.%
	7.9	8.08	13.78	1.63	0.94	2.15	0.05	0.97	0.08	-	Bal.	at.%
B	7.5	7.0	6.2	5.0	1.5	6.5	0.15	3.0	0.12	0.12	Bal.	wt.%
	7.9	8.08	13.79	1.63	0.94	2.16	0.05	0.97	0.08	0.05	Bal.	at.%

Ceramic moulds were made by the standard procedure for preparation of ceramic moulds in investment casting [14]. The primary slurry was prepared from colloidal silica as a liquid binder, with a fine-mesh refractory consisting of Al_2O_3 powder and a small amount of SiO_2 powder added according to the corresponding ratio to the mixture (stable mullite was formed). A wax pattern was dipped into the primary slurry, sprinkled with refractory stucco, and dried. The dipping-drying process was repeated several times. Finally, the wax pattern was melted out, leaving a hollow mould. The calcination temperature was 930 °C.The metal/ceramic reactions were conducted by the directional solidification method in a vacuum furnaceat 1580 °C with a vacuum less than 4 Pa.

2.2 Microstructural characterisation

Specimens were embedded in resin, ground and finely polished according to the standard metallographic preparationprocess, and ultrasonically cleaned for 30 min to remove abrasion paste from the sample surface. The microstructure at the interface between alloy and mould was characterised using field emission-scanning electron microscopy (FE-SEM; Tescan-Mira3 LMH) and analysed by energy dispersive spectroscopy (EDS). The valence states of the reaction products were determined by X-ray photoelectron spectroscopy (XPS; EscaLab250Xi). Morphologyand phase analysis on the reaction interface was carried out using focused ion-beam transmission electron microscopy (FIB-TEM; Tecnai G2 F20S-TWIN).

2.3 Thermodynamic calculations

Thermodynamic calculations were conducted in the present work to calculate the

Gibbs free energies of reactions between the ceramic moulds and REEs. Considering the segregation of elements along the interface, Gibbs free energies for the Al, La, and Y phases were obtained from the literature [18]. The Gibbs free energies for the $(La,Y)AlO_3$, $Y_3Al_5O_{12}$ and Al_2O_3 phases were calculated using thermodynamic parameters from Fabrichnaya et al. [20] according to the CALPHAD approach [21] using ThermoCalc software [22].

3. Results

3.1 Morphology characterisation

Figure 1 shows backscattered electron images (BEIs) of the interface between the two alloys and alumina-based ceramic moulds: (a) for Alloy A with 0.12 wt.%Y, and (b) for Alloy B with 0.12 wt.%Y + 0.12 wt.%La, respectively. In Fig. 1(a), a continuous interfacial reaction layer can be clearly observed, with a thickness of slightly above 10 μm (as shown as in Fig. 2(a)). There are also small areas of secondary reaction zones [23,24] and a slight amount of topologically close-packed phases (TCP) presented around the metal/ceramic interface. In Fig. 1(b), the interfacial reaction layer appears discontinuous and much thinner (as shown as in Fig. 3(a)). Instead, the secondary reaction zones are presented with γ+γ′ phases.

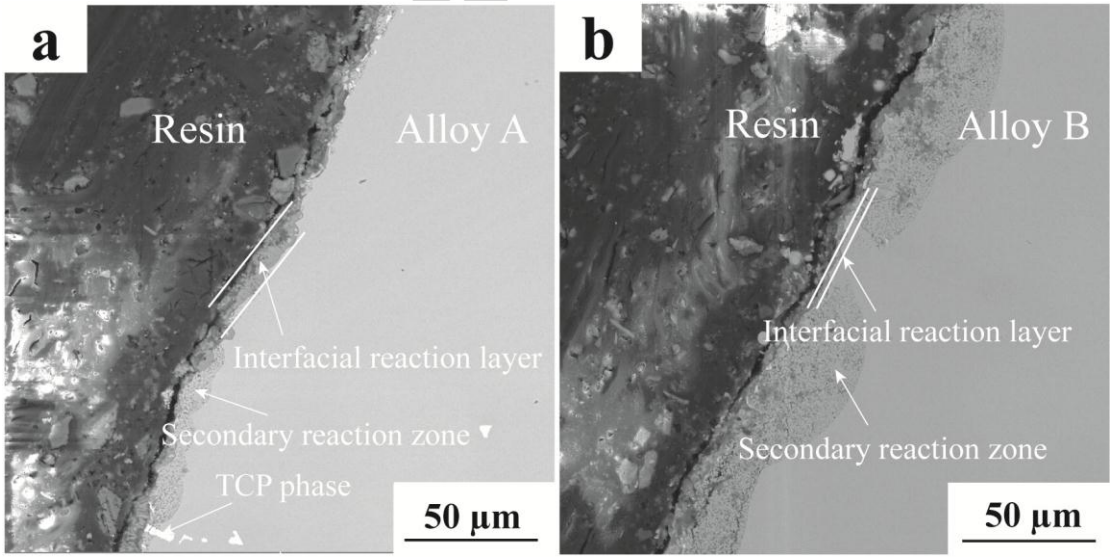

Fig. 1:BEIs of the interface between the two alloys and alumina-based ceramic moulds: (a) Alloy A with 0.12 wt.%Y; (b) Alloy B with 0.12 wt.%Y + 0.12 wt.%La.

Figure 2(a) shows a BEI of the morphology of the interfacial reaction zone for Alloy A with EDS mapping of the elements Al, Y, and O in Figs. 2(b), 2(c), and 2(d), respectively. In the interfacial reaction layer, these three elements distribute uniformly. A small region of the secondary reaction zone is located between the interfacial reaction zone and the matrix. Compositions of the three regionsin Fig. 2(a) were measured by EDS and are listed in Table 2. For region 1, the atomic ratio between Al:Y:O is approximately 5:3:12, which is consistent with the yttrium aluminium garnet (YAG) phase, $Al_5Y_3O_{12}$. In region 2, the compositions of Al and Y reach approximately 50.0 and 31.8 at.%, respectively, whereas the element O is only 11.7 at.%. The contrast of region 2 in the BEI is different from either the resin or the interfacial reaction layer, which could relate to the forming of a Y-Al binary phase in this region. The composition of region 3 is quite close to the base alloy with the absence of the added Y element, which was consumed in the reaction.

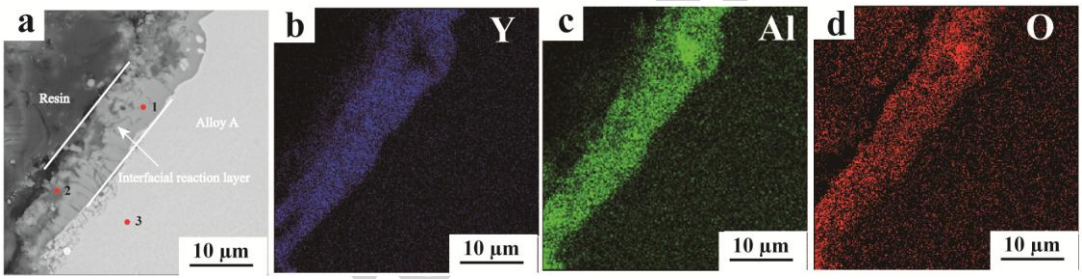

Fig. 2:BEI for the morphology of the interfacial reaction zone for Alloy A with X-ray mapping of the elements O, Al, and Y. (a) BEI; (b) element Y; (c) element Al; (d) element O.

Table 2: Compositions of the three points in Fig. 2(a) measured by EDS in at.%.

Point	O	Al	Cr	Co	Ni	Y	Mo	Hf	Ta
1	59.15	24.26	-	-	2.15	14.28	-	0.16	-
2	11.74	50.04	0.90	-	4.22	31.84	1.27	-	-
3	0.00	15.57	6.75	7.75	66.54	-	0.73	-	2.65

Figure 3(a) shows a BEI for the morphology of the interfacial reaction zone for Alloy B with EDS mapping of the elements Al, Y, La, and O in Figs. 3(b), 3(c), 3(d), and 3(e), respectively. The interfacial reaction layer is roughly 2~3 μm thick, much thinner than that of Alloy A, and elements Y and La are less homogenously distributed

in this region in comparison with those in Alloy A. Compositions of five regions in Fig. 3(a) were analysed by EDS and are listed in Table 3. The composition in regions 1, 3, and 5 contain both Y and La elements, but are rich in Y. The composition in region 4 also contains both Y and La elements, but is La-rich. Those compositions fit the YAG and lanthanum aluminium perovskite (LaAP) $LaAlO_3$ phases, respectively. Composition in region 2 is quite close to the base alloy with the absence of the added Y and La elements, which were consumed in the reaction.

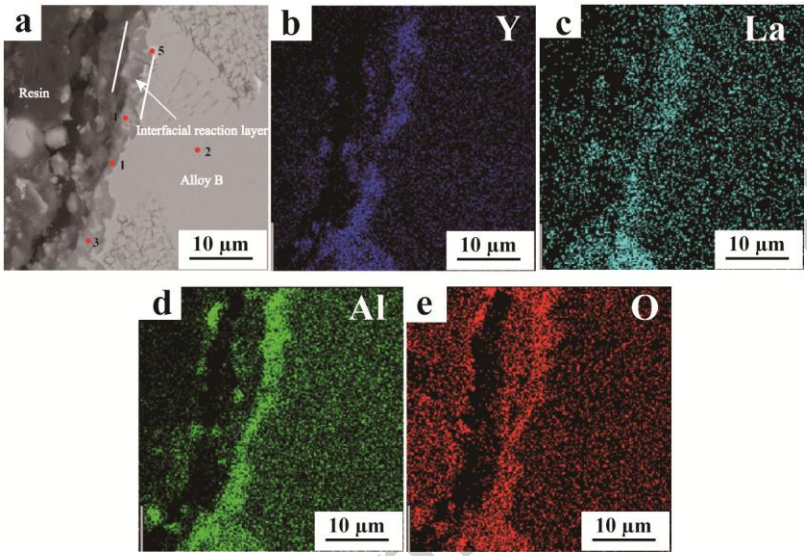

Fig. 3: Backscattered electron image for the morphology of the interfacial reaction zone for Alloy B with X-ray mapping of the elements Al, Y, La, and O. (a) BEI; (b) element Al; (c) element Y; (d) element La; (e) element O.

Table 3: Compositions of the five points in Fig. 3(a) measured by EDS in at.%.

Point	O	Al	Cr	Co	Ni	Y	Mo	La	Hf	Ta
1	52.23	30.04	-	-	2.80	13.08	-	1.85	-	-
2	-	11.89	10.93	8.84	64.85	-	1.41	-	-	2.08
3	56.16	25.91	-	-	0.99	12.76	-	4.18	-	-
4	47.78	26.70	3.40	-	4.72	5.37	-	12.03	-	-
5	59.20	19.53	-	-	4.46	8.32	-	1.53	6.97	-

3.2 Species analysis

Becausethe EDS results are semi-quantitative, XPS experiments were conducted to check the state of valence for the elements Al, Y, La, and O at the interface between the alloys and ceramic moulds. Figure 4 shows the XPS line scans along the interfacial reaction area between Alloy A and the ceramic mould. Peaks were indexed according to their binding energies [25-27]. The Y^{3+} species was identified at the binding energies of 157.5 and 159.2 eV for the YAG phase in Fig. 4(a), which is

consistent with the values of 157.23 and 159.24 eV [26] as listed in Table 4. Similar results were obtained from the XPS line scans along the interfacial reaction area between Alloy B and the ceramic mould, as shown in Fig. 5. The only difference lies in the existence of the La^{3+} species at 835.1, 838.9 / 852.4, 856.1 eV standing for the LaAP phase in Fig. 5(a), which is consistent with the values of 833.9, 838.4 / 850.7, 855.1 eV reported by Haasch et al. [27]. The species determined from their binding energies in both cases are consistent with the SEM-EDS results.

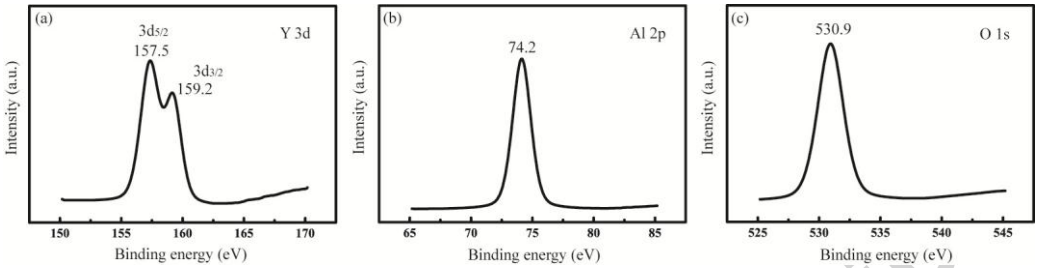

Fig. 4: XPS analysis of the interface reaction products of alloy A: (a) Y; (b) Al; (c) O.

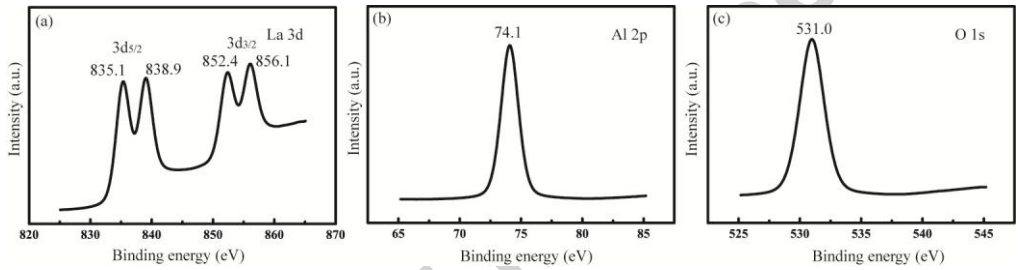

Fig. 5: XPS analysis of the interface reaction products of alloy B: (a) La; (b) Al; (c) O.

Table 4: Numerical data for XPS peaks of YAG, YAP, and LaAP phases compared with previous studies.

Phase	Element	Binding energy		
		This work	Literature data	Source
YAG	Y $3d_{5/2}$ / Y $3d_{3/2}$	157.5 / 159.2	157.23 / 159.24	[26]
	Al $2p_{3/2}$ / Al $2p_{1/2}$	74.2	73.2 / 74.13	
	O 1s	530.9	530.27	
LaAP	La $3d_{5/2}$ / La $3d_{3/2}$	835.1, 838.9 / 852.4, 856.1	833.9, 838.4 / 850.7, 855.1	[27]
	Al $2p_{3/2}$ / Al $2p_{1/2}$	74.1 / -	73.5 / -	
	O 1s	531.0	529.6	

3.3 Phase determination

The FIB-TEM technique was also employed in this study to confirm the existence of the YAG and LaAP phases. Figure 6(a) shows the FIB-selected section within the interaction region between Alloy A and the ceramic mould. A bright-field image of the sliced FIB section is shown in Fig. 6(b) showing different grains. EDS was used to

measure the compositions for regions 1 and 2; the results are listed in Table 5, indicating that both of the grains are the YAG phase. Selected area electron diffraction (SAED) patterns were taken for the two points: Fig. 6(c) and 6(d) for region 1 and Fig. 6(e) and 6(f) for region 2, respectively. The SAED patterns were indexed at the [$\bar{1}$12], [$\bar{1}$22], [001] and [012] zone axes, and it was confirmed to be the YAG phase. The lattice parameter*a*was calculated to be 1.203 nm, consistent with the literature: 1.201 nm [28].

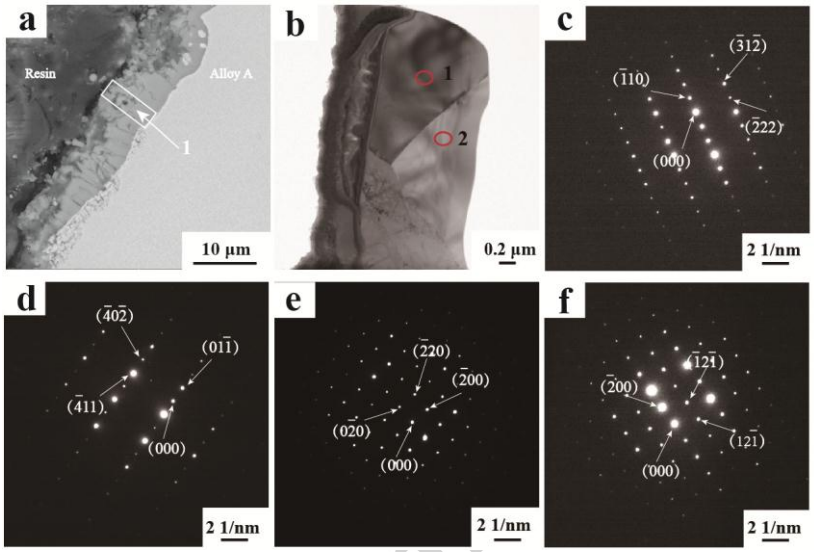

Fig.6: Bright-field TEM microstructure of the interface products between alloy A and the ceramic mould. (a) Morphologies of the interface zone; (b) TEM micrographs of the reaction products; (c), (d) SAED pattern of region1; (e), (f) SAED pattern of region 2.

Table 5: Compositions of the two points in Fig. 6(b) measured by EDS in at.%.

Point	O	Al	Cr	Ni	Y
1	60.33	26.01	0.01	0.10	13.54
2	60.26	26.27	-	0.17	13.28

For the Alloy B case, morphology at the interface is shown in Fig. 7(a), where a rectangle is added to illustrate where the FIB sections were obtained. The BEIs of the two sections are shown in Figs. 7(b) and 7(e), the compositions of which were identified by EDS as the LaAP and YAG phases listed in Table 6. By indexing the diffraction patterns of Figs. 7(c) and 7(d) referring to Fig. 7(b), the zone axes of [01$\bar{1}$2] and [$\bar{4}$223], respectively, were obtained for the LaAP phase. The lattice parameters *a* and *c* were calculated to be 0.534 and 1.296 nm, respectively, which fit the literature data well, *a*=0.537 nm and *c*=1.310 nm [29]. The SAED patterns for Fig. 7(e) are

shown in Figs. 7(f) and 7(g). The zone axis indexes are $[\bar{1}22]$ and $[01\bar{1}]$ for the YAG phase, and the lattice parameter is 1.203 nm, similar to the reported values of 1.201 nm [28].

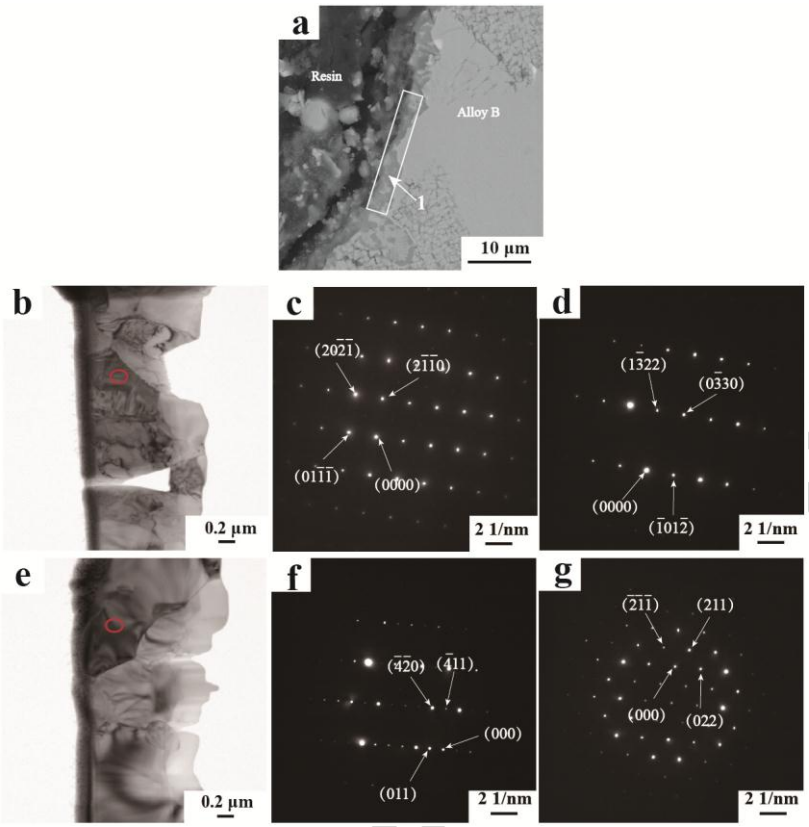

Fig.7: Bright-field TEM microstructure of the interface products between Alloy B and an Al_2O_3 base mould. (a) Morphologies of the interface zone; (b), (e) TEM micrographs of the reaction products; (c), (d) SAED pattern of the reaction zone in(b); (f), (g) the SAED pattern of the reaction zone in(e).

Table 6: Compositions of the two points in Fig. 7(b) measured by EDS in at.%.

Point	O	Al	Cr	Ni	Mo	Y	La
1 Fig. 7(b)	52.34	22.88	1.93	0.60	1.80	3.34	17.07
2 Fig. 7(e)	56.88	28.78	-	0.10	-	14.15	0.06

4. Discussion

From Fig. 2(a) and Fig. 3(a), it appears that the interfacial reaction layer of Alloy A with 0.12%Y is thicker and continuous; the layer of the Alloy B with 0.12%Y+0.12%La is thinner and discrete (in wt.%). This implies that the additional La additives reduce the thickness ofthe interfacial reaction layer between alloy and ceramics.

According to the analysis of SEM-EDS, XPS, and FIB-TEM, it was confirmed that for Alloy A with 0.12 wt.% Y, the YAG phase forms at the interface; for Alloy B with 0.12 wt.% Y +0.12 wt.% La, both YAG and LaAP phases form at the interface. The interfacial reactions between REEs and alumina are

$$\frac{4}{3}Al_2O_3+Y\rightarrow\frac{1}{3}Y_3Al_5O_{12}+Al \quad (1)$$

$$Al_2O_3+La\rightarrow LaAlO_3+Al \quad (2)$$

Note that Eq. (1) comes from coupling the two reactions $\frac{1}{2}Al_2O_3+\frac{1}{2}Y\rightarrow\frac{1}{2}Y_2O_3+Al$ and $\frac{5}{6}Al_2O_3+\frac{1}{2}Y_2O_3\rightarrow\frac{1}{3}Y_3Al_5O_{12}$; Eq. (2) is from coupling $\frac{1}{2}Al_2O_3+La\rightarrow\frac{1}{2}La_2O_3+Al$ and $\frac{1}{2}Al_2O_3+\frac{1}{2}La_2O_3\rightarrow LaAlO_3$. This shows that 1 mol of Y will consume 4/3 mol of alumina, but 1 mol of La will consume only 1 mol of alumina. This cannot explain why adding La and Y simultaneously can reduce interfacial reactions, given that both elements can react with alumina. The Gibbs free energies of formation (ΔG) for the reactions were also calculated against temperature [18,20] and are plotted in Fig. 8. The Gibbs free energies of formation of Eq. (1) are much lower than those of Eq. (2). Therefore, when adding La and Y at the same time, Y is still prone to react first. Hence, something could have been missing from the perspective of the Gibbs free energies of formation (ΔG).

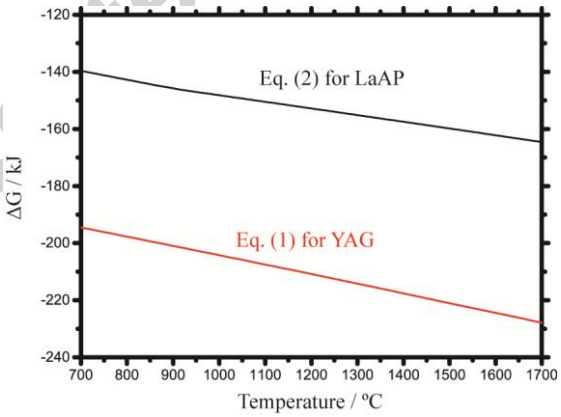

Fig.8:ΔG-T diagram of interface reactions (1) and (2) between alloy and mould.

In light of the calculated Al_2O_3-Y_2O_3-La_2O_3 isothermal sections at 1600 °C shown in Fig. 9 [20], there is very small solubility of La in the YAG phase, but such solubility has not been detected as shown in Tables 2 and 5. And a fair amount of

solubility of Y in the LaAP phase has been measured. This indicates that some of the Y element may dissolve into the LaAP phase, which is indeed detected by EDS in region 4 in Table 3 and region 1 in Table 6. The shifts of XPS peaks were also detected and are presentedin Figure 5 and Table 4. Therefore, Eq. (2) should be modified to the following:

$$Al_2O_3+(La,Y)_{Liq}\rightarrow(La,Y)AlO_3+Al \quad (3)$$

The Gibbs free energies of formation of the $(La,Y)AlO_3$ phase instead of the $LaAlO_3$ phase were then calculated using the CALPHAD approach and are plotted in Fig. 10, which can be used to compare to that of the YAG phase [20]. Note that the (La,Y)Liq is a solution phase modelled as ideal solution, since there are no thermodynamic assessment of La-Y system, while phase diagram indicated continuous solid and liquid solutions [30]. Because the lowest solubility of Y in the $LaAlO_3$ phase is suggested as 3.34 at.% (region 1 in Table 6), the Gibbs free energy of formation of the LaAP phase was calculated under the solubility of Y in the LaAP of 3, 3.4, and 4 at.%. Figure 10 shows that when the solubility of Y in the LaAP phase is 3 at.%, the Gibbs free energy of formation of the LaAP phase is still higher than that of the YAG phase, $\Delta G^{LaAP}>\Delta G^{YAG}$. However, when the solubility of Y reaches 3.4 at.%, the situation is reversed, $\Delta G^{LaAP}<\Delta G^{YAG}$. For the solubility of Y of 4 at.%, the Gibbs free energy of formation of the LaAP phase is much lower than that of the YAG phase. This means that when La and Y are simultaneously added, Y atoms favour dissolving into the LaAP phase rather than reacting with the alumina phase to form YAG. Those dissolved Y elements are not prone to participate in interfacial reactions with the ceramic moulds, and this explains the synergetic effect of La and Y on retarding the interfacial reactions. What needs to be pointed out is that the reactions written in the paper do not include any Ni. Including of Ni will make phase relations much more complicated and all presented calculations may be not relevant.

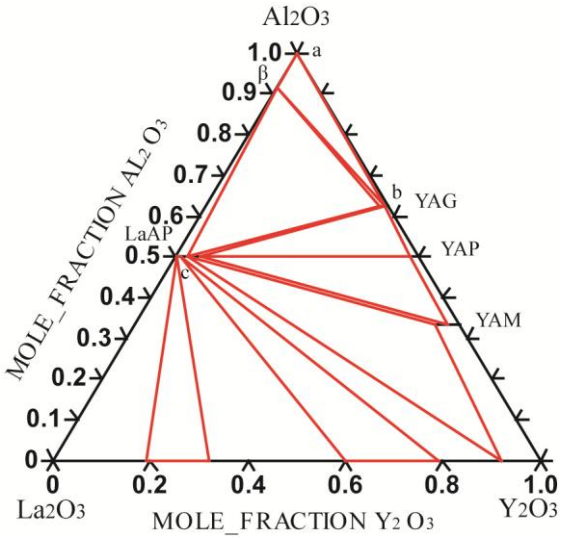

Fig. 9: A calculated phase diagram of the Al_2O_3-La_2O_3-Y_2O_3 system at 1600 °C [20].

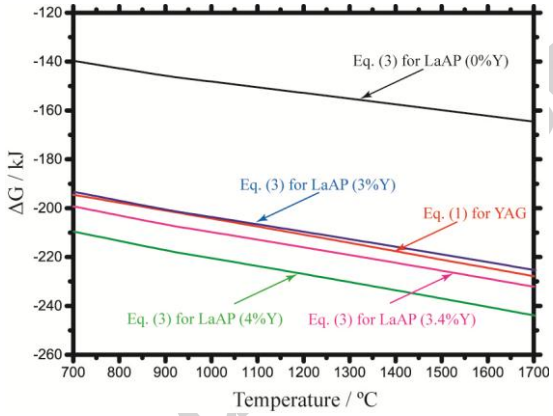

Fig.10:ΔG-T diagram of interface reactions (1) and (3) between alloy and mould.

Furthermore, the local phase equilibrium at the interface of Alloy A is Al_2O_3 + YAG (ab line in Fig. 9). When adding La and Y at the same time, the local phase equilibrium is changed to be LaAP + YAG (bc line in Fig. 9). The diffusion path from the Al_2O_3 phase to the LaAP + YAG phase region is via either YAG or β-$LaAl_{11}O_{18}$. This reduces the reaction rate between REEs and ceramic moulds. This would be helpful to minimise defects at the interface between Ni-based single-crystal superalloys and ceramic moulds during casting.

Additionally, the element Al isconsumed during the interfacial reaction of Alloy A as stated in Eq. (1); thus, there is not a large secondary reaction zone observed in Fig. 1(a). However, there are some Al atoms (γ' stabiliser) produced and expelled into the

alloy matrix during the interfacial reaction of Alloy B (see Eqs. (2) and (3)); it is thus prone to form a secondary reaction zone with γ+γ′ phases as shown in Fig. 1(b). This is beyond the scope of the present work, but would beinteresting to further investigate in the future.

5. Conclusions

Interfacial reactions between a second-generationNi-based single-crystal superalloy with rare earth elements Y and Y+La and alumina-based moulds were investigated in terms of morphology, microstructure, and thermodynamics. Adding Y and La simultaneously has the synergetic effect of retarding reactions between reactive REEs and the ceramic moulds. SEM-EDS, XPS, and FIB-TEM results confirm the formation of the LaAP phase with some Y dissolved when adding La. Thermodynamic calculations indicate that when La and Y are present at the same time, Y favours dissolvinginto the LaAP phase, rather than reacting with the mould material. This study provides some hints on minimising casting defects during the manufacture of single-crystal Ni-based alloys using alumina-based moulds.

Acknowledgement

This work was financially supported by National Natural Science Foundation of China (Grant No. 51761014, 51401095, 51501229) and the Jiangxi Provincial Department of Science and Technology (Grant No. 20171BAB216004, 20161BBH80030).

References

[1] Rolls-Royce, The Jet engine, the Key Publish Limited, 2005.

[2] Reed RC, The Superalloys: Fundamentals and applications, Cambridge University Press, 2006.

[3] Chmiela B, Roskosz S, Non-metallic inclusions in castings made of nickel-base superalloys, Solid State Phenomena, 2014, 212: 211-214.

[4] Zeng Q, Zhang DT, Ma SW, Zhang Y, Cao LM, The study on the boundary condition between Al_2O_3 mould and a new type single crystal superalloy with Re, Journal of Materials Engineering, 2001, 5: 20-21.

[5] Yao SJ, Tang DZ, Liu XG, Li X, Wang LL, Cao CX, Ding FZ, Chen H, Interface reaction between DD6 single crystal superalloy and ceramic mold, Journal of Aeronautical Materials, 2015, 35: 1-7.

[6] Chen XY, Xiao L, Yu JB, Sun BD, Li F, Research status of the interface reactions between superalloys and ceramic materials in investment casting, Special Casting and Nonferrous Alloys, 2016, 36: 844-848.

[7] Li Q, Song JX, Wang DG, Yu Q, Xiao CB, Effect of Cr, Hf and temperature on interface reaction between nickel melt and silicon oxide core, Rare Metals, 2013, 30: 405-409.

[8] Chen XY, Jin Z, Bai XF, Zhou YZ, Jin T, Sun XF, Effect of C on the interfacial reaction and Wettability between a Ni-based superalloy and ceramic mould, ActaMetallurgicaSinica, 2015, 51: 853-858.

[9] Zheng L, Xiao CB, Zhang GQ, Gu GH, Li X, Liu XG, Xue M, Tang DZ, Investigation of interfacial reaction between high Cr content cast nickel based superalloy K4648 and ceramic cores, Journal of Aeronautical Materials, 2012, 32: 10-22.

[10] Valenza F, Muolo ML, Passerone A, Wetting and interactions of Ni- and Co-based superalloys with different ceramic materials, Journal of Materials Science, 2010, 45: 2071-2079.

[11] Yao JS, Tang DZ, Liu XG, Xiao CB, Li X, Cao CX, Interaction between two ni-base alloys and ceramic moulds, Materials Science Forum, 2013, 747-748:

765-771.

[12] Chen XY, Zhou YZ, Zhang CW, Jin T, Sun XF, Effect of Hf on the interfacial reaction between a Ni base superalloy and a ceramic material, ActaMetallurgicaSinica, 2014, 50: 1019-1024.

[13] Wang LL, Li JR, Tang DZ, Liu SZ, Interfacial reactions between SiO_2-ZrO_2 ceramic core and DZ125, DD5, DD6 casting superalloys, Journal of Materials Engineering, 2016, 44: 9-14.

[14] Li JR, Xiong JC, Tang DZ, Advanced high temperature structural materials and technology, National Defense Industry Press, 2003.

[15] Xue M, Study on ceramic-superalloy interface reactions during the directional solidification processing,Thesis, Tsinghua University, 2007.

[16] Ford DA, Fullagar KPL, Bhangu HK, Thomas MC, Burkholder PS, Korinko PS, Harris K, Wahl JB, Improved performance rhenium containing single crystal alloy turbine blades utilizing ppm level of the highly reactive elements lanthanum and yttrium, Transactions of the ASME: Journal of Engineering for Gas Turbines and Power, 1999, 121: 138-143.

[17] Harris K, Wahl JB, Improved single crystal superalloys, CMSX-4(SLS)[La+Y] and CMSX-486, Superalloys 2004, 2004: 45-52.

[18] Scientific Group Thermodata Europe, SGTE pure element database, www.sgte.net, 2001.

[19] Callister, Jr., WD, Rethwisch DG, Fundamentals of materials science and engineering: An integrated approach, 4th Edition, Wiley, 2012.

[20]Fabrichnaya O, Savinykh G, Schreiber G, Phase relations in the ZrO_2-La_2O_3-Y_2O_3-Al_2O_3 system: experimental study and thermodynamic modelling, Journal of the European Ceramic Society, 2013, 33:37-49.

[21] Spencer PJ, A brief history of CALPHAD, CALPHAD, 2008, 32: 1-8.

[22] Andersson J-O, Helander T, Höglund L, Shi P, Sundman B, Thermo-Calc&dictra, computational tools for materials science, CALPHAD, 2002, 26: 273-312.

[23] D'souza N, Welton D, West GD, Edmonds IM, Wang H, On the role of oxidation and vaporisation in surface micro-structural instability during solution heat treatment

of Ni-base superalloys, Metallurgical and Materials Transactions A, 2014, 45:5968-5981.

[24] D'souza N, Welton D, Wang H, Implications of solute super-saturation in growth of vaporisation induced recrystallised grains during heat treatment in Ni-base superalloys, International Journal of Materials Research, 2015, 106: 288-295.

[25] Wagner CD, Handbook of X-ray photoelectron spectroscopy, Perkin-Elmer, Eden Prairie, MN, 1979.

[26] Pawlak DA, Woz´niak K, Frukacz Z, Barr TL, Fiorentino D, Seal S, ESCA Studies of Yttrium Aluminium Garnets, Journal of Physical Chemistry B, 1999, 103: 1454-1461.

[27] Haasch RT, Breckenfeld E, Martin LW, Single crystal perovskitesanalyzed using X-ray photoelectron spectroscopy: 3. $LaAlO_3$(001), Surface Science Spectra, 2014, 21: 103-111.

[28] Shimony Y, Kalisky Y, Lotem H, Goldbart Z, Kagan J, Growth and characterization of (Ho,Tm,Er):YAG crystals for 2.09 μm laser, Journal of Applied Physics, 1990, 68: 2966-2971.

[29] Li J, Smith AE, Jiang P, Stalick JK, Sleight AW, Subramanian MA, True composition and structure of hexagonal "$YAlO_3$", Actually $Y_3Al_3O_8CO_3$, Inorganic Chemistry, 2015, 54: 837-844.

[30] K.A. Gschneidner Jr., F.W. Calderwood, The La-Y (Lanthanum-Yttrium) system, Bulletin of Alloy Phase Diagram, 1982, 3: 94–96.

List of table captions

List of figure captions